Ali, Shahjahan; Hosoda, Takashi; Kimura, Ichiro

Study on Spatial Distributions and Topological Change of Turbulent Structures in Coherent Vortices with a Non-Linear K-e Model

STUDY ON SPATIAL DISTRIBUTIONS AND TOPOLOGICAL CHANGE OF TURBULENT STRUCTURES IN COHERENT VORTICES WITH A NON-LINEAR k–ε MODEL

Md. Shahjahan Ali [1], Takashi Hosoda [2], and Ichiro Kimura[3]

[1] Phd Student, Department of Urban Management, Kyoto University
Nishikyoku, Kyodai Katsura Campus, C1-3, Kyoto 615-8540, Japan, e-mail: bablu41@yahoo.com
[2] Professor, Department of Urban Management, Kyoto University
Nishikyoku, Kyodai Katsura Campus, C1-3, Kyoto 615-8540, Japan, e-mail: hosoda@mbox.kudpc.kyoto-u.ac.jp
[3]Associate Professor, Faculty and Graduate School of Engineering, Hokkaido University
Nishi-8, Kita-13, Kita-ku, Sapporo, 060-8623, Japan, e-mail: i-kimu2@eng.hokudai.ac.jp

ABSTRACT

Coherent structures are an intrinsic feature of many turbulent flows that are often observed in many natural and man-made engineering applications. The work presented in this paper can be classified into twofold. In the first part, the spatial distributions and topological change of turbulent structures in an idealized vortex street are investigated using the analytical approach. In the second part, the 3D numerical simulation is carried out for the flow field of a compound open channel to generate the horizontal vortices at the interface of main channel and flood plain. The formation of singular points in the coherent structures, and the topological change of turbulent structures with the singular points are investigated. It is observed that the turbulent structures are changed spatially depending on the structures of singular points (i.e. vortex and saddle points). The topological change of turbulent structures in the horizontal vortices of the compound channel is found to be consistent with that of approximate solution of the ideal vortex street.

Keywords: compound channel, stuart vortex, non-linear k–ε model, RANS

1. INTRODUCTION

Flows with large scale vortices due to shear layer instability are often observed in many natural, geophysical as well as anthropogenic activities. In turbulent shear flows, they play a vital role in the overall development of flow through the entrainment, mixing and momentum exchange between fast and slow speed fluids. Figure 1 shows an example of the span wise cut of coherent structure, in particular in the plane mixing layer. The outer contour of coherent vorticity denotes the structure boundary. It shows that there are two critical points in the structure: the saddle (S) characterized by negligible spanwise vorticity, and the center of vortex (C) characterized by peak spanwise vorticity. Based on the experimental results on turbulent structures of a plane shear layer, Hossain (1986) reported that the structure of turbulent normal stresses at vortex point are elliptical in shape; on the other hand, the turbulent shear stresses show hyperbolic profile. The same patterns are also confirmed in further studies with turbulent axisymmetric jets and wakes.

Among the turbulence models, the k–ε model is the most popular and frequently adopted one (Jaw and Chen, 1998). However, the standard k–ε model cannot produce satisfactory results for the flow field having high rate of strain and rotation because of its isotropic assumption of eddy viscosity. On the other hand, a non-linear model is capable of handling the rotational effects as well as anisotropy of turbulence. Since, this type of model

has been using for calculating many turbulent flows that contain vorticity in the flow field, it is worthy to examine the non-linear models predictability of turbulent structures in an ideal vortex street.

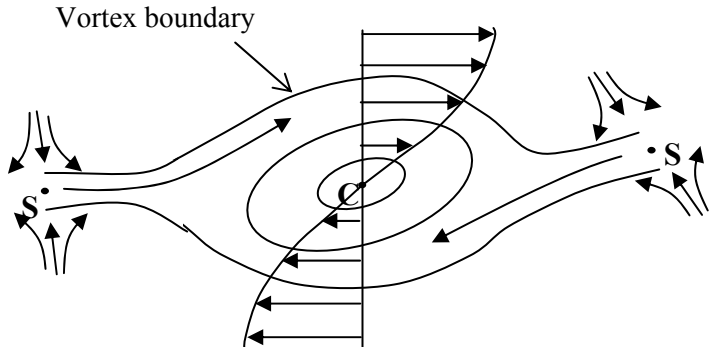

Figure 1 Sketch of a coherent vortex in plane mixing layer

The work presented in this paper can be classified into twofold. In the first part, an approximate solution is derived for turbulent characteristics of an ideal vortex street. The Stuart vortex, which contains both vortex and saddle patterns in its vorticity contour, is considered for this analysis. The aim is to explore the model applicability to large scale vortices, and to investigate the spatial topological change of turbulent structures with singular points.

In a compound channel, the large scale vortices are formed at the interface of main channel and flood plain. Although the vortex characteristics in a compound channel are studied by many researchers both in experimental and numerical means, all are concentrated mainly on the effect of vortices on cross-sectional flow or turbulence profiles as well as on the channel resistance properties. However, as far as authors' knowledge, the spatial change of turbulent structures with the singular points of large scale vortices are not reported for compound open channel flows. In this study, 3D numerical simulation is carried out for the flow field of a compound open channel to generate the coherent horizontal vortices at the interface of main channel and flood plain. The formations of singular points (i.e. vortex and saddle patterns) in the coherent structures, and the topological change of turbulent structures with the singular points are investigated.

2. GOVERNING EQUATIONS

The 3D equations for the k–ε model can be expressed as follows:

Continuity equation:
$$\frac{\partial U_i}{\partial x_i} = 0 \tag{1}$$

Momentum equation:
$$\frac{\partial U_i}{\partial t} + \frac{\partial U_j U_i}{\partial x_j} = g_i - \frac{1}{\rho}\frac{\partial P}{\partial x_i} + \frac{\partial}{\partial x_j}\left(-\overline{u_i u_j}\right) + \nu \frac{\partial^2 U_i}{\partial x_j{}^2} \tag{2}$$

k - equation:
$$\frac{\partial k}{\partial t} + \frac{\partial k U_j}{\partial x_j} = -\overline{u_i u_j}\frac{\partial U_i}{\partial x_j} + \frac{\partial}{\partial x_j}\left\{\left(\frac{\nu_t}{\sigma_k} + \nu\right)\frac{\partial k}{\partial x_j}\right\} - \varepsilon \tag{3}$$

ε - equation:
$$\frac{\partial \varepsilon}{\partial t} + \frac{\partial \varepsilon U_j}{\partial x_j} = -c_{\varepsilon 1}\frac{\varepsilon}{k}\overline{u_i u_j}\frac{\partial U_i}{\partial x_j} + \frac{\partial}{\partial x_j}\left\{\left(\frac{\nu_t}{\sigma_\varepsilon} + \nu\right)\frac{\partial \varepsilon}{\partial x_j}\right\} - c_{\varepsilon 2}\frac{\varepsilon^2}{k} \tag{4}$$

In standard k–ε model, the Reynolds stresses are determined as Eq. (5).

$$-\overline{u_i u_j} = \nu_t S_{ij} - \frac{2}{3}k\delta_{ij}, \nu_t = C_\mu \frac{k^2}{\varepsilon}, C_\mu = 0.09 \tag{5}$$

In this study, a 2nd order non-linear model expressed in Eq. (6) is used, where C_μ and C_β are considered as a function of strain (S) and rotation (Ω) parameters.

$$-\overline{u_i u_j} = \nu_t S_{ij} - \frac{2}{3}k\delta_{ij} - \frac{k}{\varepsilon}\nu_t \sum_{\beta=1}^{3} C_\beta \left(S_{\beta ij} - \frac{1}{3} S_{\beta\alpha\alpha}\delta_{ij} \right) \tag{6}$$

here,

$$\nu_t = C_\mu \frac{k^2}{\varepsilon}, \quad S_{ij} = \frac{\partial U_i}{\partial x_j} + \frac{\partial U_j}{\partial x_i}, \quad \Omega_{ij} = \frac{\partial U_i}{\partial x_j} - \frac{\partial U_j}{\partial x_i}, S = \frac{k}{\varepsilon}\sqrt{\frac{1}{2}S_{ij}S_{ij}}, \Omega = \frac{k}{\varepsilon}\sqrt{\frac{1}{2}\Omega_{ij}\Omega_{ij}} \tag{7}$$

In Eq. (6),

$$S_{1ij} = \frac{\partial U_i}{\partial x_\gamma}\frac{\partial U_j}{\partial x_\gamma}, \quad S_{2ij} = \frac{1}{2}\left(\frac{\partial U_\gamma}{\partial x_i}\frac{\partial U_j}{\partial x_\gamma} + \frac{\partial U_\gamma}{\partial x_j}\frac{\partial U_i}{\partial x_\gamma} \right), \quad S_{3ij} = \frac{\partial U_\gamma}{\partial x_i}\frac{\partial U_\gamma}{\partial x_j} \tag{8}$$

$$C_\mu = \frac{c_{\mu o}\,(1 + c_{ns}S^2 + c_{n\Omega}\Omega^2)}{1 + c_{ds}S^2 + c_{d\Omega}\Omega^2 + c_{ds\Omega}S\Omega + c_{ds1}S^4 + c_{d\Omega 1}\Omega^4 + c_{ds\Omega 1}S^2\Omega^2} \tag{9}$$

$$C_\beta = c_{\beta o}\frac{1}{1 + m_{ds}S^2 + m_{d\Omega}\Omega^2} \tag{10}$$

Here, σ_k= 1.0, σ_ε= 1.3, $c_{\varepsilon 1}$ = 1.44 $c_{\varepsilon 2}$ = 1.92, c_{10}=0.40, c_{20}=0.0 and c_{30}= -0.13, have their standard values.

Table 1 shows two sets of model constants. The actual values of model constants in C_μ and C_β determined in our previous studies (Ali et al., 2006) are given in Run-1. Run-2 shows a set of trial values that will be used to investigate the sensitivity of empirical functions to the structural change of turbulent properties in the vortex point (Focus).

Table 1 Estimated (Run-1) and trial (Run-2) values of model constants

Model Const.	$\mathbf{c_{\mu 0}}$	$\mathbf{c_{ns}}$	$\mathbf{c_{n\Omega}}$	$\mathbf{c_{ds}}$	$\mathbf{c_{ds\Omega}}$	$\mathbf{c_{d\Omega}}$	$\mathbf{c_{ds1}}$	$\mathbf{c_{d\Omega 1}}$	$\mathbf{c_{ds\Omega 1}}$	$\mathbf{m_{ds}}$	$\mathbf{m_{d\Omega}}$
Run-1	0.09	0.005	0.0068	0.008	-0.003	0.004	0.00005	0.00005	0.00025	0.01	0.003
Run-2	0.09	0.01	0.007	0.008	-0.003	0.004	0.00005	0.00005	0.00025	0.01	0.003

3. APPRPXIMATE SOLUTION OF STUART VORTICES

The equation for stream function of the Stuart vortex can be expressed as follows:

$$\psi = \log(\cosh y + A\ \cos x) \tag{11}$$

here, $0 \geq A \geq -1$ is a constant and indicates the eccentricity of the elliptical streamline of the vortex. A moderate eccentricity of A=- 0.5 is used in this calculation. Although Stuart vortex is a solution of Euler equation, it is shown that the turbulence can be generated in the fixed flow field of this vortex.

The stream function of Stuart vortex is expanded using the Taylor's function, near the origin (0, 0) and at a periodic distance of (π, 0), for the flow field of vortex center and saddle point, respectively. The approximated stream functions for focus and saddle points are given in Eqs. (12) and (13), respectively. Their stream-line contours are shown in Figure 2.

$$\psi_{focus} = \ln\left(1/2\right) + \frac{1}{2}x^2 + y^2 - \frac{1}{6}x^4 - \frac{1}{2}x^2y^2 - \frac{5}{12}y^4 + \ldots\ldots \tag{12}$$

$$\psi_{saddle} = \ln\left(1/2\right) - \frac{1}{6}x^2 + \frac{1}{3}y^2 + \frac{1}{18}x^2y^2 - \frac{1}{36}y^4 + \ldots\ldots \tag{13}$$

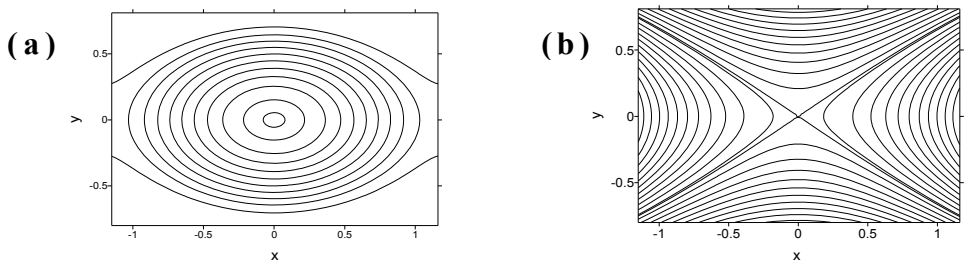

Figure 2 Streamline contour of Stuart vortex approximated by Taylor function at (a) vortex center (focus) (b) saddle point

3.1 Turbulent structures at vortex center (Focus)

From Eq. (12), the velocity field for the vortex point is calculated as

$$U_x = \frac{\partial \psi}{\partial y} = 2y - x^2 y - \frac{5}{3}y^3, \quad U_y = -\frac{\partial \psi}{\partial x} = -x + xy^2 + \frac{2}{3}x^3 \tag{14}$$

In order to determine turbulent stresses using Eq. (6), we need to know the distribution of turbulent kinetic energy (k) and dissipation rate (ε). The following polynomial functional forms are assumed for the distributions of k and ε.

$$k = k_{00} + k_{01}x + k_{10}y + k_{02}x^2 + k_{20}y^2 + k_{11}xy \tag{15}$$

$$\varepsilon = \varepsilon_{00} + \varepsilon_{01}x + \varepsilon_{10}y + \varepsilon_{02}x^2 + \varepsilon_{20}y^2 + \varepsilon_{11}xy \tag{16}$$

here, k_{00}, k_{01}, k_{10}, k_{02}, k_{20}, k_{11} are the unknown coefficients for k; and ε_{00}, ε_{01}, ε_{10}, ε_{02}, ε_{20}, ε_{11} are that for ε distributions respectively.

Substituting the assumed k and ε distributions [Eqs. (15) and (16)] into k–ε equations [Eqs.(3) and (4)], the following algebraic expressions are derived considering the relations among the coefficients for the same power of variables (x, y) in each equation. To avoid the complexity in solving a large number of equations, the higher order terms of k_{01}, k_{10}, k_{02}, k_{20}, k_{11}, ε_{01}, ε_{10}, ε_{02}, ε_{20} and ε_{11} are neglected to form a set of linear equations.

k-equation:

$$0: \quad c_{\mu_0} k_{00}^2 (1)_0 - (2)_0 + \frac{c_{\mu_0}}{\sigma_k} k_{00}^2 \{2k_{02} + 2k_{20}\}(1)_0 = 0 \tag{17}$$

$$x: \quad k_{10} = A_f k_{01} + B_f \varepsilon_{01} \tag{18}$$

$$y: \quad 2k_{01} = A_f k_{10} + B_f \varepsilon_{10} \tag{19}$$

$$x^2: \quad -k_{11} = A_f k_{02} + B_f \varepsilon_{02} + C_{f5}(k_{02} + k_{20}) + C_{f1} \tag{20}$$

$$y^2: \quad 2k_{11} = A_f k_{20} + B_f \varepsilon_{20} - C_{f6}(k_{02} + k_{20}) + C_{f2} \tag{21}$$

$$xy: \quad 4k_{02} - 2k_{20} = A_f k_{11} + B_f \varepsilon_{11} \tag{22}$$

ε -equation:

$$0: \quad c_{\varepsilon_1} c_{\mu_0} k_{00}^2 \varepsilon_{00}^2 (1)_0 - c_{\varepsilon_2} \varepsilon_{00}^2 (2)_0 + \frac{c_{\mu_0}}{\sigma_\varepsilon} k_{00}^3 \{2k_{02} + 2k_{20}\}(1)_0 = 0 \tag{23}$$

$$x: \quad -\varepsilon_{10} = C_f k_{01} + D_f \varepsilon_{01} \tag{24}$$

$$y: \quad 2\varepsilon_{01} = C_f k_{10} + D_f \varepsilon_{10} \tag{25}$$

$$x^2: \quad -\varepsilon_{11} = C_f k_{02} + D_f \varepsilon_{02} + C_{f7}(\varepsilon_{02} + \varepsilon_{20}) + C_{f3} \tag{26}$$

$$y^2: \quad 2\varepsilon_{11} = C_f k_{20} + D_f \varepsilon_{20} - C_{f8}(\varepsilon_{02} + \varepsilon_{20}) + C_{f4} \tag{27}$$

$$xy: \quad 4\varepsilon_{02} - 2\varepsilon_{20} = C_f k_{11} + D_f \varepsilon_{11} \tag{28}$$

here,

$$A_f = \left[c_{\mu_0}\varepsilon_{00}k_{00}^3\left\{(1)_0(2m_{ds}+18m_{d\Omega})+(4)_0(2c_{ns}+18c_{n\Omega})\right\}+2c_{\mu_0}\varepsilon_{00}k_{00}(1)_0(4)_0 - \varepsilon_{00}k_{00}(2)_0(2m_{ds}+18m_{d\Omega})-\varepsilon_{00}k_{00}(4)_0-\varepsilon_{00}k_{00}(4)_0\left\{\varepsilon_{00}^2(2c_{ds}+6c_{ds\Omega}+18c_{d\Omega}) + 4k_{00}^2(c_{ds1}+9c_{ds\Omega1}+81c_{d\Omega1})\right\}\right]/\left\{(2)_0(4)_0\right\}$$

$$B_f = \left[2c_{\mu_0}\varepsilon_{00}^2k_{00}^2\left\{(1)_0+(4)_0\right\}+c_{\mu_0}k_{00}^2(1)_0(4)_0-\left\{2(2)_0\varepsilon_{00}^2+4\varepsilon_{00}^4(4)_0 + \varepsilon_{00}^2k_{00}^2(4)_0(2c_{ds}+6c_{ds\Omega}+18c_{d\Omega})+(2)_0(4)_0\right\}\right]/\left\{(2)_0(4)_0\right\}$$

$$C_f = \left[c_{\mu_0}c_{\varepsilon_1}\varepsilon_{00}^2k_{00}^3\left\{(1)_0(2m_{ds}+18m_{d\Omega})+(4)_0(2c_{ns}+18c_{n\Omega})\right\}+2c_{\mu_0}c_{\varepsilon_1}\varepsilon_{00}^2k_{00}(1)_0(4)_0 - c_{\varepsilon_2}\varepsilon_{00}^2k_{00}(2)_0(2m_{ds}+18m_{d\Omega})-c_{\varepsilon_2}\varepsilon_{00}^2k_{00}(4)_0\left\{\varepsilon_{00}^2(2c_{ds}+6c_{ds\Omega}+18c_{d\Omega}) + 4k_{00}^2(c_{ds1}+9c_{ds\Omega1}+81c_{d\Omega1})\right\}\right]/\left\{(2)_0(4)_0k_{00}\right\}$$

$$D_f = \left[2c_{\mu_0}c_{\varepsilon_1}\varepsilon_{00}^3k_{00}^2\left\{(1)_0+(4)_0\right\}+2c_{\mu_0}c_{\varepsilon_1}\varepsilon_{00}k_{00}^2(1)_0(4)_0-c_{\varepsilon_2}\left\{2(2)_0\varepsilon_{00}^2+4\varepsilon_{00}^5(4)_0 + \varepsilon_{00}^3k_{00}^2(4)_0(2c_{ds}+6c_{ds\Omega}+18c_{d\Omega})+\varepsilon_{00}(2)_0(4)_0\right\}\right]/\left\{(2)_0(4)_0k_{00}\right\}$$

$$C_{f1} = \left[-\varepsilon_{00}k_{00}^2\left\{(2)_0(2m_{ds}-18m_{d\Omega})+\varepsilon_{00}^2(4)_0(2c_{ds}-18c_{d\Omega})\right\}+2c_{\mu_0}\varepsilon_{00}k_{00}^2(1)_0(4)_0 + c_{\mu_0}\varepsilon_{00}k_{00}^4(1)_0(2m_{ds}-18m_{d\Omega})+\varepsilon_{00}k_{00}^4(4)_0\left\{c_{\mu_0}(2c_{ns}-18c_{n\Omega})+4(c_{ds1}-81c_{d\Omega1})\right\}\right]/\left\{(2)_0(4)_0\right\}$$

$$C_{f2} = \left[-\varepsilon_{00}k_{00}^2\left\{(2)_0(-8m_{ds}-36m_{d\Omega})-\varepsilon_{00}^2(4)_0(8c_{ds}+36c_{d\Omega}+18c_{ds\Omega})\right\}-8c_{\mu_0}\varepsilon_{00}k_{00}^2(1)_0(4)_0 + c_{\mu_0}\varepsilon_{00}k_{00}^4(1)_0(-8m_{ds}-36m_{d\Omega})+\varepsilon_{00}k_{00}^4(4)_0\left\{c_{\mu_0}(-8c_{ns}-36c_{n\Omega}) - 4(4c_{ds1}+162c_{d\Omega1}-27c_{ds\Omega1})\right\}\right]/\left\{(2)_0(4)_0\right\}$$

$$C_{f3} = \left[-c_{\varepsilon_2}\varepsilon_{00}^2k_{00}^2\left\{(2)_0(2m_{ds}-18m_{d\Omega})+\varepsilon_{00}^2(4)_0(2c_{ds}-18c_{ds\Omega})\right\}+2c_{\mu_0}c_{\varepsilon_1}\varepsilon_{00}^2k_{00}^2(1)_0(4)_0 + c_{\mu_0}c_{\varepsilon_1}\varepsilon_{00}^2k_{00}^4(1)_0(2m_{ds}-18m_{d\Omega})+\varepsilon_{00}^2k_{00}^4(4)_0\left\{c_{\varepsilon_2}c_{\mu_0}(2c_{ns}-18c_{n\Omega}) + 4c_{\varepsilon1}(c_{ds1}-81c_{d\Omega1})\right\}\right]/\left\{(2)_0(4)_0\right\}$$

$$C_{f4} = \left[-c_{\varepsilon_2}\varepsilon_{00}^2k_{00}^2\left\{(2)_0(-8m_{ds}-36m_{d\Omega})-\varepsilon_{00}^2(4)_0(8c_{ds}+36c_{d\Omega}+18c_{ds\Omega})\right\}-8c_{\mu_0}c_{\varepsilon_1}\varepsilon_{00}^2k_{00}^2(1)_0(4)_0 + c_{\mu_0}c_{\varepsilon_1}\varepsilon_{00}^2k_{00}^4(1)_0(-8m_{ds}-36m_{d\Omega})+\varepsilon_{00}^2k_{00}^4(4)_0\left\{c_{\mu_0}c_{\varepsilon_1}(-8c_{ns}-36c_{n\Omega}) - 4c_{\varepsilon_2}(4c_{ds1}+162c_{d\Omega1}-27c_{ds\Omega1})\right\}\right]/\left\{(2)_0(4)_0k_{00}\right\}$$

$$C_{f5} = \left[\frac{2c_{\mu_0}}{\sigma_k}-\varepsilon_{00}k_{00}^4\left\{(1)_0(2m_{ds}-18m_{d\Omega})+(4)_0(2c_{ns}-18c_{n\Omega})\right\}\right]\Big/\left\{(2)_0(4)_0\right\}$$

$$C_{f6} = \left[\frac{2c_{\mu_0}}{\sigma_k}-\varepsilon_{00}k_{00}^4\left\{(1)_0(8m_{ds}+36m_{d\Omega})+(4)_0(8c_{ns}+36c_{n\Omega})\right\}\right]\Big/\left\{(2)_0(4)_0\right\}$$

$$C_{f7} = \left[\frac{2c_{\mu_0}}{\sigma_\varepsilon}-\varepsilon_{00}k_{00}^4\left\{(1)_0(2m_{ds}-18m_{d\Omega})+(4)_0(2c_{ns}-18c_{n\Omega})\right\}\right]\Big/\left\{(2)_0(4)_0\right\}$$

$$C_{f8} = \left[\frac{2c_{\mu_0}}{\sigma_\varepsilon}-\varepsilon_{00}k_{00}^4\left\{(1)_0(8m_{ds}+36m_{d\Omega})+(4)_0(8c_{ns}+36c_{n\Omega})\right\}\right]\Big/\left\{(2)_0(4)_0\right\}$$

$$(1)_0 = \varepsilon_{00}^2+c_{ns}k_{00}^2+9c_{n\Omega}k_{00}^2,\quad (2)_0 = \varepsilon_{00}^2\left(\varepsilon_{00}^2+c_{ds}k_{00}^2+3c_{ds\Omega}k_{00}^2+9c_{d\Omega}k_{00}^2\right)+k_{00}^4\left(c_{ds1}+9c_{ds\Omega1}+81c_{d\Omega1}\right)$$

$$(4)_0 = \varepsilon_{00}^2+m_{ds}k_{00}^2+9m_{d\Omega}k_{00}^2$$

Solving the twelve equations from Eqs. (17) to (28), twelve unknowns are determined in terms of model constants. Substituting the obtained values of unknown coefficients into Eqs. (15) and (16), the k and ε profiles are calculated. The distributions of turbulent intensities and shear stresses are obtained by non-linear constitutive equations.

Figure 3 shows the turbulent structures at the center of vortex determined by approximate solution using the model constants of Run-1. It is observed that, the profiles for turbulent kinetic energy (k), dissipation rate (ε) [Figures (a) and (b)] as well as the turbulent

normal stresses in x, y and z directions, expressed as $\overline{u_1u_1}$, $\overline{u_2u_2}$ and $\overline{u_3u_3}$ respectively, [Figures (c), (d) and (e)] show elliptical structures; on the other hand the turbulent shear stress in xy plane ($\overline{u_1u_2}$) show hyperbolic (saddle pattern) profile [Figure (f)] at the center of vortex. These features are consistent with the previous experiments reported for free shear flows.

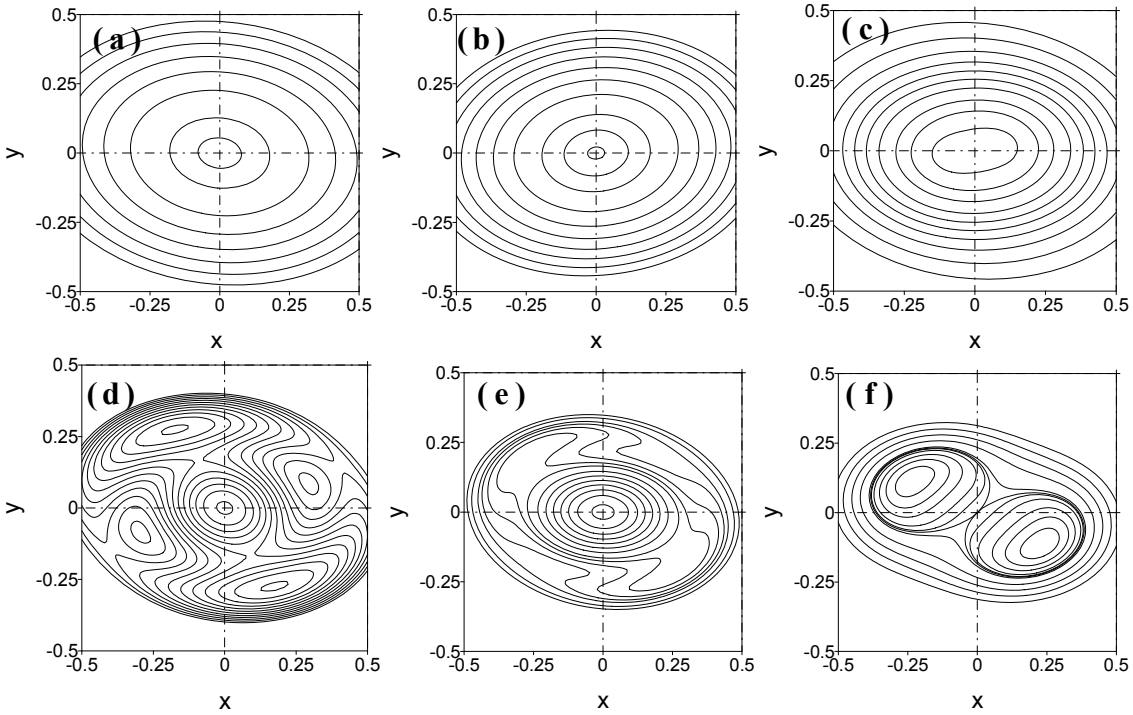

Figure 3 Turbulent structures by approximate solution for vortex point (Run-1):
(a) k (b) ε (c) $\overline{u_1u_1}$ (d) $\overline{u_2u_2}$ (e) $\overline{u_3u_3}$ (f) $\overline{u_1u_2}$

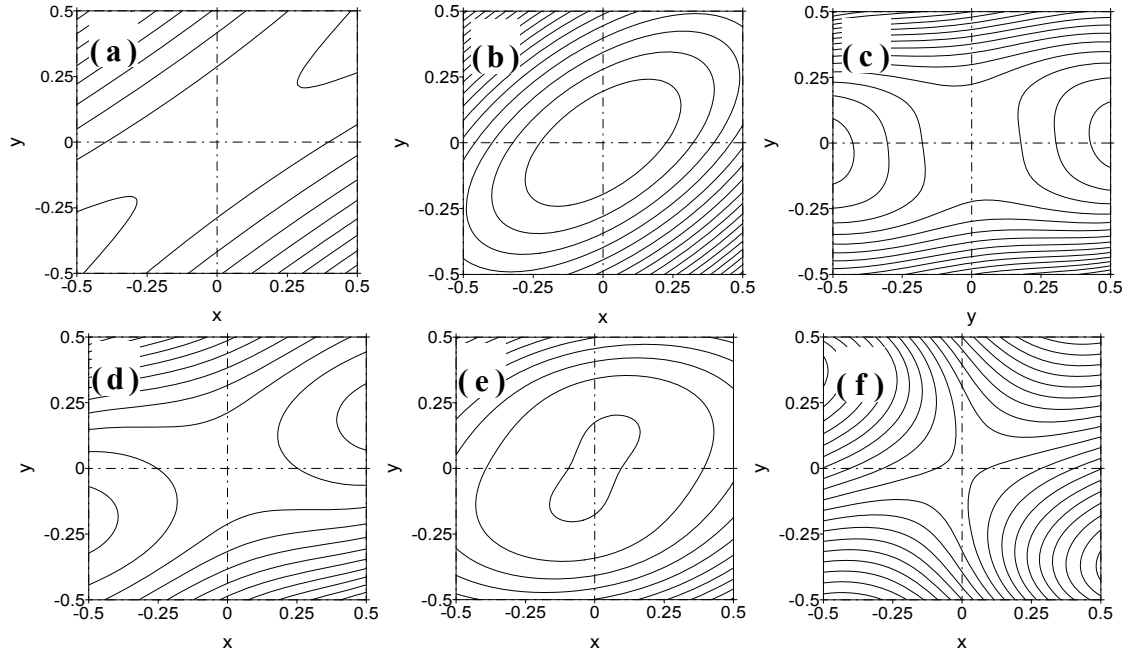

Figure 4 Turbulent structures by approximate solution for vortex point (Run-2):
(a) k (b) ε (c) $\overline{u_1u_1}$ (d) $\overline{u_2u_2}$ (e) $\overline{u_3u_3}$ (f) $\overline{u_1u_2}$

The set of model constants for Run- 2 is a trial set of model constants to investigate the

influence of functional form of C_μ on turbulent structures. Figure 4 shows the turbulent structures at vortex center predicted by Run-2. It is observed that the turbulent kinetic energy (k), and turbulent intensities, $\overline{u_1u_1}$ and $\overline{u_2u_2}$, show hyperbolic profile instead of elliptical structures. That means, Run-2 fails to predict the actual turbulent structures that observed in previous experimental studies. By comparing the results for two set of model constants, it can be concluded that the turbulent structures in a vortex is sensitive to the functional form of C_μ.

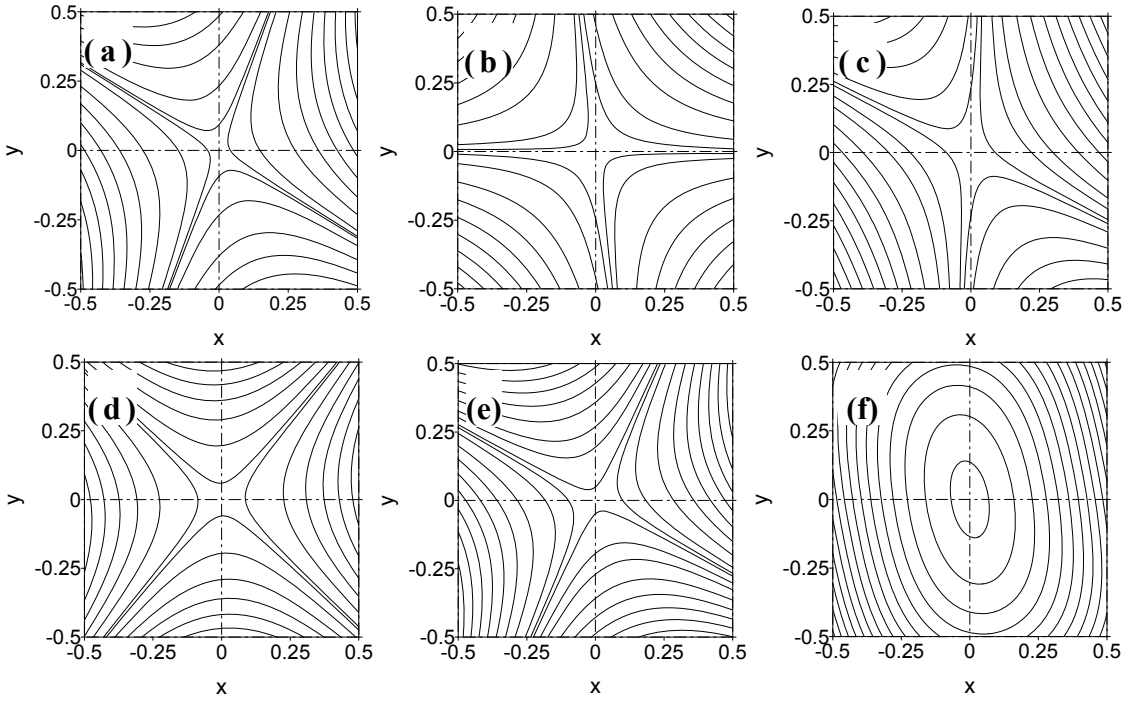

Figure 5 Turbulent structures by approximate solution at saddle point (Run-1):
(a) k (b) ε (c) $\overline{u_1u_1}$ (d) $\overline{u_2u_2}$ (e) $\overline{u_3u_3}$ (f) $\overline{u_1u_2}$

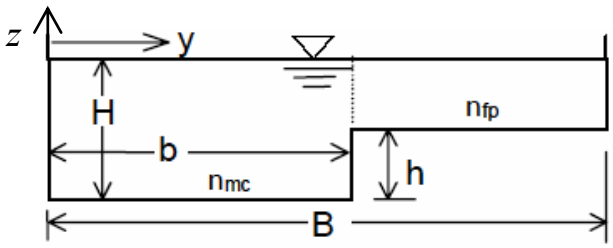

Figure 6 Cross-section of compound open channel

3.2 Turbulent structures at Saddle point

Applying the same procedure as vortex point (Focus) described in last section, the turbulent structures are calculated for saddle point using the stream function given in Eq. (13). The calculated profiles for k, ε and turbulent stresses are shown in Figure 5. It is observed that the turbulent energy, dissipation rate and turbulent normal stresses show hyperbolic profile (saddle pattern) in a saddle point. However, the shear stress shows elliptical structure.

From analytical solution, it can be concluded that the turbulent structures are changed with the spatial distance depending on the structure of singular points. The turbulent normal stresses show elliptical profiles near vortex center, which changed to hyperbolic profile near

saddle point at a stream-wise periodic distance of π. However, the shear stresses show hyperbolic structure at vortex center and changes to elliptical at saddle point. The spatial change of turbulent structures for turbulent kinetic energy and dissipation rates are found similar to turbulent normal stresses. These features are consistent with the previous experiments of coherent vortices in plane shear layer and turbulent jets (Hossain, 1986).

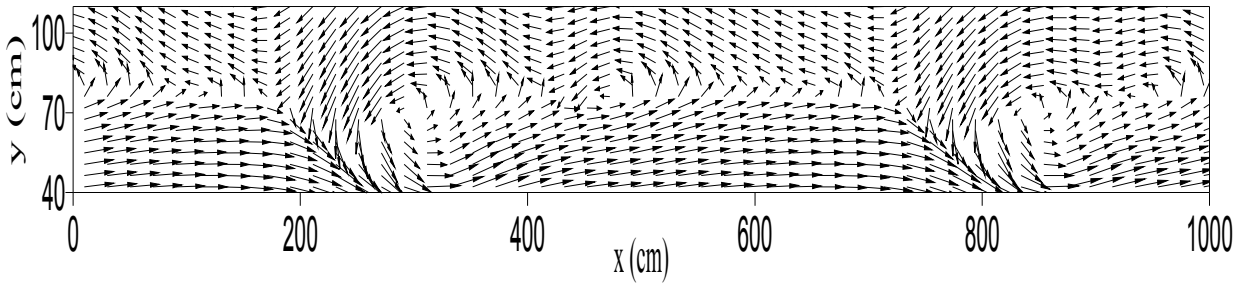

Figure 7 Plan view of flow vector showing the horizontal vortices at the interface of main channel and flood plan (a part of flow domain is shown at t =300 sec)

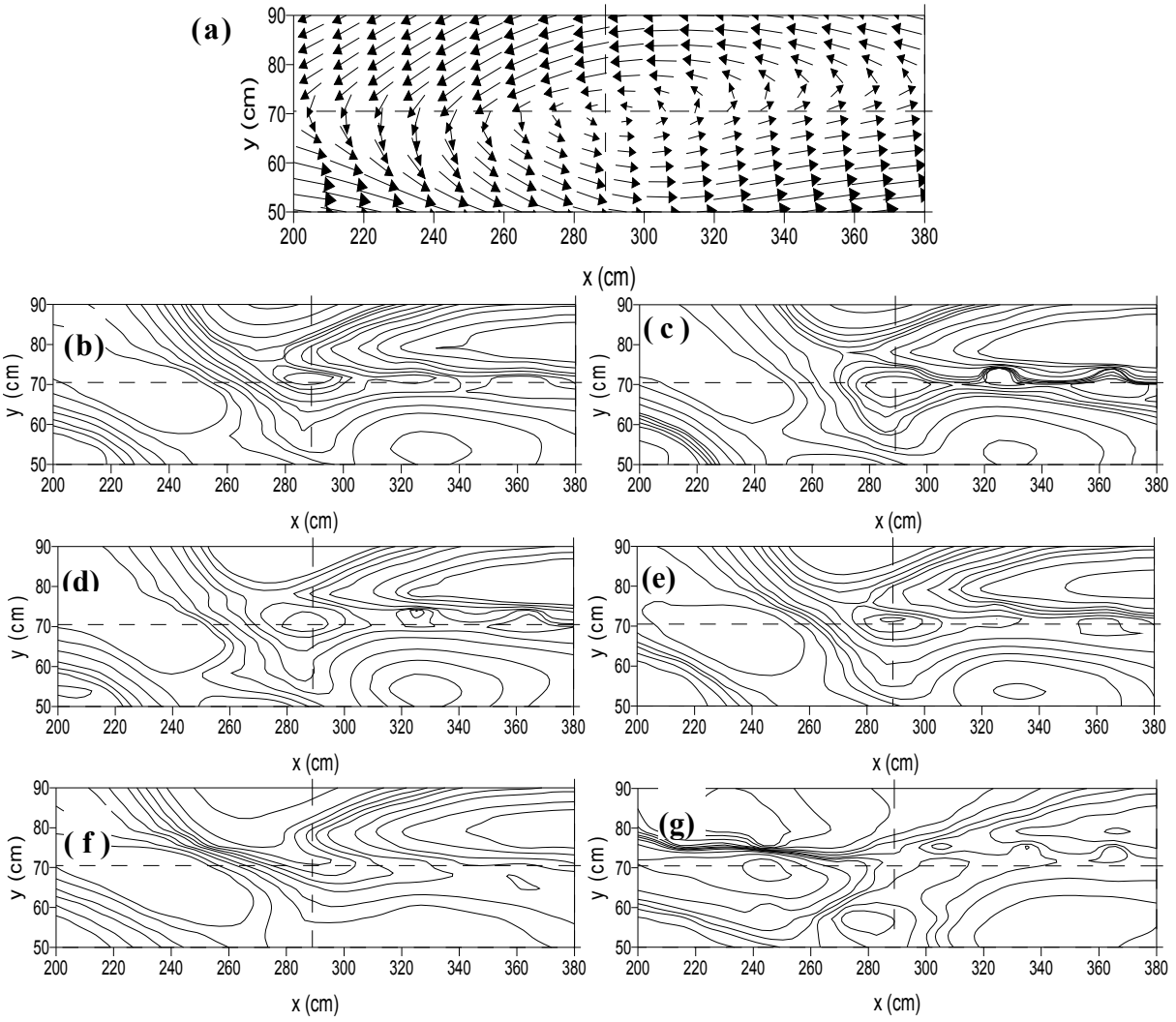

Figure 8 Turbulent structures near the center of a vortex (x =200~380 cm): (a) plan view of flow vectors (b) k (c) ε (d) $\overline{u_1 u_1}$ (e) $\overline{u_2 u_2}$ (f) $\overline{u_3 u_3}$ (g) $\overline{u_1 u_2}$

4. LARGE SCALE VORTICES IN COMPOUND CHANNEL

The code solves the governing equations for mean velocities and turbulent flow field discretized with the finite volume method and is based on a staggered grid system. The cross-section of the flume is shown in Figure 6. The computational domain is consist of 200 grids in longitudinal (stream-wise, x), 42 in transverse (width-wise, y) and 11 in vertical (depth-wise, z) directions. The hydraulic variables shown in Figure 6 are B=200, b=75.5, H=7.5 and h=5 cm with a longitudinal slope of 1/1000. n_{mc} (= 0.01) and n_{fp} (= 0.028) denote the Manning's roughness coefficient for main channel and flood plain, respectively. Since the present work is mainly focused on the modeling of large scale vortices, the averaged flow properties are not included here. However, the simulation details and the predictability of present model to the mean flow properties can be found in Ali et al. (2007).

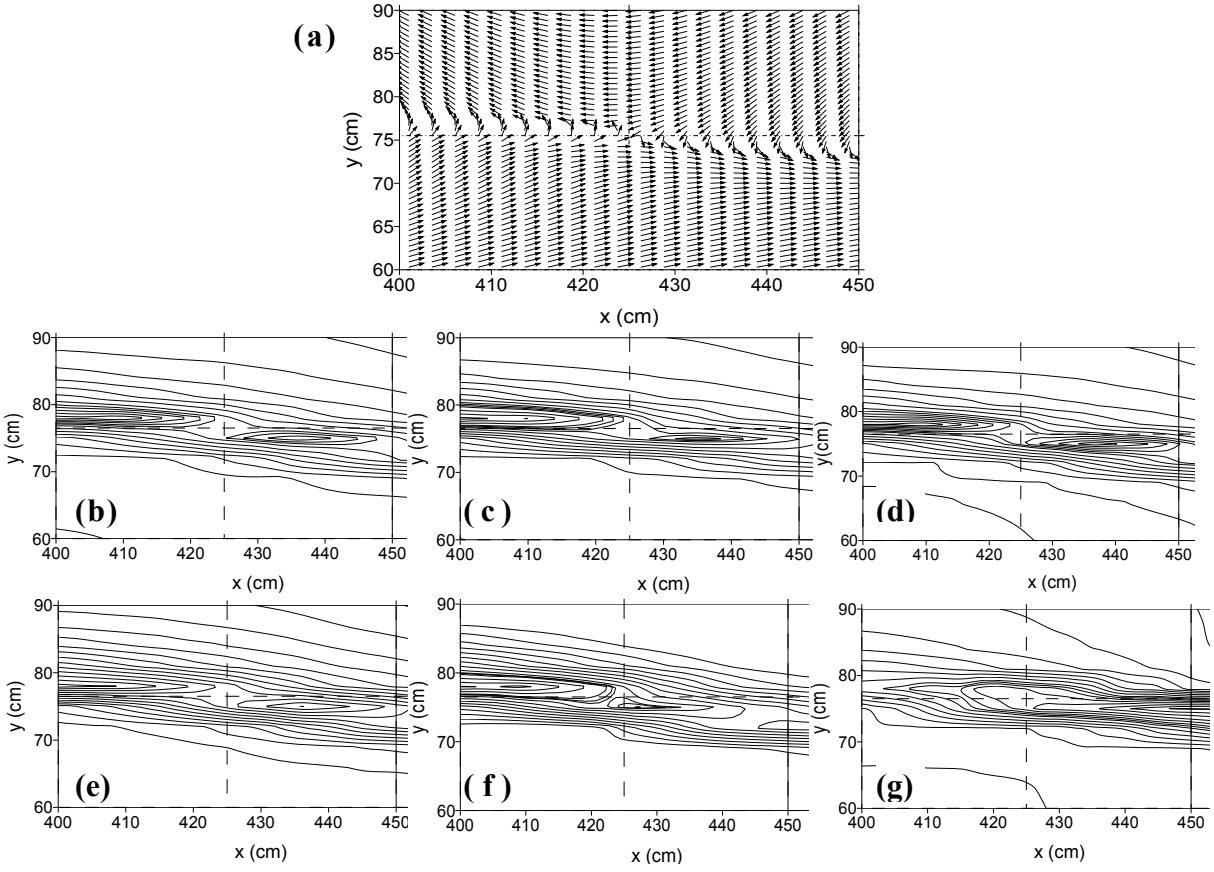

Figure 9 Turbulent structures near the saddle point (x =400~450 cm): (a) plan view of flow vector, (b) k (c) ε (d) $\overline{u_1u_1}$ (e) $\overline{u_2u_2}$ (f) $\overline{u_3u_3}$ (g) $\overline{u_1u_2}$

Figure 7 shows the plan view (horizontal) of simulated flow vectors near the interface region at t=300 sec. The focus and saddle patterns in the generated coherent vortices are observed in this figure clearly. The turbulent structures for a vortex point (focus) is shown in Figure 8 for the stream-wise distance of 200 to 380 cm. The flow vectors of individual vortex is shown in Figure 8(a). The figure indicates that the turbulent normal stresses in x, y and z directions, expressed as $\overline{u_1u_1}$, $\overline{u_2u_2}$ and $\overline{u_3u_3}$ respectively, show the contours in elliptical structure at the vortex center. The structures of turbulent kinetic energy (k) and dissipation rate (ε) are similar to turbulent normal stresses. On the other hand, the turbulent shear stress in xy plane ($\overline{u_1u_2}$) shows hyperbolic profile. The results are well agreed to the approximate

solutions of turbulent structures in an ideal vortex street.

The turbulent structures for a saddle point are shown in Figure 9. It is observed that the turbulent energy and dissipation rate as well as turbulent normal stresses show hyperbolic profile (saddle pattern) in a saddle point. However, the shear stress shows elliptical structure. Therefore, the changes of topological structures of turbulent stresses in the large scale vertices of a compound channel are found compatible to the analytical solution of the ideal vortex street, and hence, to the available experimental studies on free shear flows.

It is also found that the turbulence productions follow the structures of turbulent shear stresses. The quantitative comparison indicates that the turbulence production at the vortex center is very small, but is larger in the upstream and downstream directions, being the maximum at the saddle on either side. This feature is also consistent with the previous experiments of coherent structures in free shear flows.

5. CONCLUSION

Based on a non-linear k–ε model, approximate solutions are derived for the turbulent properties of an idealized vortex street to examine the predictability of the model for large scale vortices. The unsteady 3D numerical simulations are also carried out for a compound channel, and the spatial change of turbulent structures with singular points are investigated. The findings are summarized below :

- The Stuart vortex, which contains both vortex and saddle patterns in its vorticity contour, is considered as an ideal simple vortex street. The turbulent structures of the vortex street are found to be sensitive to the functional form of the coefficient of eddy viscosity, C_μ.
- The turbulent structures are found to be changed with the spatial distance depending on the structures of singular points. It is observed that the turbulent normal stresses show elliptical structure near vortex center, which changes to hyperbolic profile near saddle point at a stream-wise periodic distance of π. However, the shear stress show hyperbolic structures at vortex center, and the structure changes to elliptical at saddle point.
- The topological change of turbulent kinetic energy and dissipation rates with stream-wise spatial distance are found similar to the turbulent normal stresses.
- The model is found to be capable of generating the horizontal vortices at the interface of main channel and flood plain.
- The turbulent structures in horizontal vortices observed at the interface of main channel and flood plain are well agreed with that of approximate solutions of an ideal vortex street and consistent with previous experimental observations of coherent structures in free shear flows.

REFERENCES

Ali, M. S., Hosoda, T., Kimura, I., Onda, S. (2006), Approximate solution of an axisymmetric swirling jet using non-linear k–ε model with consideration of realizability, *Journal of Applied Mechanics, JSCE,* vol. 9, pp. 821-832.

Ali, M. S., Hosoda, T. and Kimura, I. (2007), Unsteady RANS computations of compound channel flows with large scale vortices and secondary currents, *5th International symposium on Environmental Hydraulics,* ASU, Tempe, Arizona.

Hossain, A. K. M. F. (1986), Coherent structures and turbulence, *J. Fluid. Mech.,* 173, pp. 303-356.

Jaw, S.Y. and Chen, C. J. (1998), Present status of second order closure turbulence models. I: overview, *J. Engg. Mech.*, ASCE. 124, pp.485-501.